ЖЭТФ, 2013, том 143, вып. 4, стр. 759–769 

# KINETIC SIMULATIONS OF ARGON DUSTY PLASMA AFTERGLOW INCLUDING METASTABLE ATOM KINETICS

*A. L. Alexandrov**, *I. V. Schweigert*, *D. A. Ariskin*

*Institute of Theoretical and Applied Mechanics, Siberian Branch of the Russian Academy of Sciences*
*630090, Novosibirsk, Russia*

Received July 16, 2012

The afterglow of a dusty plasma of rf discharge in argon is simulated by Particles In Cells–Monte Carlo Collisions (PIC–MCC) method. The experimental observation that heavy dust contamination of plasma leads to an anomalous increase in the electron density at the beginning of afterglow is explained by release of electrons from the dust surface. Under the assumption that the floating potential of particles is in equilibrium with plasma conditions, the fast cooling of electrons in afterglow plasma due to a rapid escape of hot electrons from the volume leads to a decrease in the magnitude of the floating potential and hence to a loss of charge by dust. The intensive desorption of electrons from nanoparticles is the origin of anomalous behavior of the electron density. At the next stage of afterglow, when the electrons become cool, the plasma decay is defined by ambipolar diffusion. The effect of metastable argon atoms is also considered. Additional ionization due to metastable atom collisions affects the electron temperature but does not change the behavior of the electron density qualitatively.

**DOI**: 10.7868/S0044451013040150

## 1. INTRODUCTION

The afterglow of dusty plasma is an interesting field of investigation due to the complexity of various nonequilibrium processes that occur in an unsteady plasma containing charged nanoparticles after switching off the discharge [1–5]. In the experiment [1], the anomalous behavior of electron density was observed, namely, a fast increase in the electron density in the dusty plasma of the radio-frequency (rf) discharge immediately after switching off the discharge voltage. The release of electrons from charged dust particles was suggested as a possible explanation. Analytic approaches to the description of the processes in a dusty afterglow plasma [4, 5] are usually restricted to the case of weak dust contamination, when the dust space charge is small compared to the electron density (small Havnes parameter). The anomalous electron density behavior is observed in the opposite case of heavy dust contamination.

In [3], other possible mechanisms leading to the anomalous electron density increase were suggested, such as ion–dust and metastable–dust secondary electron emission, and the ionization due to metastable argon atom collisions. The release of electrons from dust particles was not considered, because the authors of [3] stated that the dust discharging rate is defined by the work function of the nanoparticle material (4–5 eV for carbonaceous dust). On the other hand, it was suggested in [6, 7] that the electrons are kept on the nanoparticle surface by a self-induced short-range polarization potential and hence the electron binding energy is much less than 1 eV and the characteristic time of dust discharging is of the order of 1 $\mu$s. This allows assuming that the electrons adsorbed on dust can be released quickly and the dust floating potential can vary rapidly enough to be in equilibrium with the local plasma environment even during the early afterglow.

A promising approach is to study the afterglow by direct simulation of ion and electron motion, in particular, by the Particles In Cells–Monte Carlo Collisions (PIC–MCC) method, which is applicable for plasma with a large Havnes parameter. In this paper, the afterglow of rf discharge in heavy dusted plasma is considered using the PIC–MCC method, with the simplifying assumption that the dust particle floating potential is in equilibrium with the plasma environment and at each instant is defined by the equality of electron and

*E-mail: a_alex@itam.nsc.ru

ion currents to the particle surface. The kinetics of metastable argon atoms is also taken into consideration.

## 2. DUSTY DISCHARGE MODEL

The rf discharge and the afterglow plasma in argon are simulated by the conventional PIC–MCC technique. The PIC–MCC model of high-frequency discharge dusty plasma is based on the electron and ion kinetic equations, including their interaction with dust nanoparticles and the Poisson equation. In this model, the velocity distribution functions of electrons, $f_e(t, x, \mathbf{v})$, and ions, $f_i(t, x, \mathbf{v})$, in the approximation of three-dimensional velocity space and one-dimensional real space are obtained by numerically solving the Boltzmann equations

$$\frac{\partial f_e}{\partial t} + \mathbf{v}_e \frac{\partial f_e}{\partial x} - \frac{e\mathbf{E}}{m_e} \frac{\partial f_e}{\partial \mathbf{v}_e} = J_e, \qquad n_e(t,x) = \int f_e d\mathbf{v}_e, \tag{1}$$

and

$$\frac{\partial f_i}{\partial t} + \mathbf{v}_i \frac{\partial f_i}{\partial x} + \frac{e\mathbf{E}}{m_i} \frac{\partial f_i}{\partial \mathbf{v}_i} = J_i, \qquad n_i(t,x) = \int f_i d\mathbf{v}_i, \tag{2}$$

where $v_e$, $v_i$, $n_e$, $n_i$, and $m_e$, $m_i$ are respectively the electron and ion velocities, densities, and masses, $\mathbf{E}$ is the electric field, and $J_e$ and $J_i$ are the collision integrals for electrons and ions, which include elastic and inelastic collisions with the background gas and negatively charged dust particles.

The electron and ion kinetics in the PIC–MCC model is simulated with test particles with weight $W$, which is the number of electrons or ions represented by this test particle. The equations of motion are integrated for electrons and ions in the discharge electric field accounting for the collisions with neutral atoms and negatively charged dust. The probabilities of elastic and inelastic scattering events during an electron/ion time step are set by the cross sections depending on the test particle energy. If an ionization event occurs, the new electron and ion test particles with the same coordinates and weights are introduced. The test particle leaving the calculation area through the electrodes or captured by dust is excluded from the simulation. The interelectrode gap is covered with a calculation grid (one-dimensional in this case). The macroscopic characteristics of the plasma such as the electron and ion average energies $n_e$ and $n_i$ are calculated by integrating the electron and ion distribution functions over the calculation grid nodes. The electric field in plasma is calculated at each time step from the Poisson equation

$$\Delta\phi = 4\pi e \left[n_e - n_i + Z_d(x) n_d(x)\right], \quad E = -\frac{d\phi}{dx}, \tag{3}$$

where $n_e$ and $n_i$ are obtained from the PIC–MCC calculation. The boundary conditions are the sinusoidal applied voltage on one electrode and zero voltage on the other, grounded electrode. The space charge of the dust particles with the density $n_d(x)$ and the mean particle charge $Z_d(x)$, depending on the spatial coordinate, are included. The particle charge and density are found self-consistently during the simulation, as described below.

The cross sections for electron–argon reactions are taken from [8]. For argon ions, the resonant charge exchange is taken into account. The influence of dust in this model is included similarly to how this was done in the models in [9–11]. In the kinetic simulation, the cross sections of electron and ion capture by dust particles are included, which are taken from the Orbital Motion Limit (OML) theory:

$$\sigma_{ed} = \begin{cases} \pi r_d^2 (1 + eU_d/\varepsilon_e), & \varepsilon_e > -eU_d, \\ 0, & \varepsilon_e < -eU_d, \end{cases}$$

$$\sigma_{id} = \pi r_d^2 (1 - eU_d/\varepsilon_i),$$

where $U_d = -eZ_d/r_d$ is the (negative) floating potential of the dust particle surface gained in the discharge plasma, $\varepsilon_e$ and $\varepsilon_i$ are the kinetic energy of electrons and ions, $r_d$ is the radius of the dust particle, $Z_d$ is the particle charge number, and $e$ is the elementary charge. The value of the floating potential $U_d$ must provide equal electron and ion fluxes to the dust surface, thus making the particles charge steady. We used two methods of finding the $U_d$ in the discharge simulation. The first was to control the number of ions and electrons collected by dust according to the mentioned collision cross sections and adjust the value of $U_d$ to make them equal. The other method, more efficient for simulation of afterglow with rapidly changing plasma parameters, was to use analytic expressions for the electron and ion fluxes onto a dust particle, derived from the OML theory (see, e. g., [12]):

$$I_e = \pi n_e r_d^2 v_{T_e} \exp\left(\frac{eU_d}{kT_e}\right), \qquad I_i = \pi n_i r_d^2 v_{T_i} \left(1 - \frac{eU_d}{kT_i}\right), \tag{4}$$

where $n_e$ and $n_i$ are local electron and ion densities, $T_e$ and $T_i$ are their temperatures, all taken from the PIC–MCC simulation, $k$ is the Boltzmann constant, and $v_{T_e}$ and $v_{T_i}$ are thermal velocities, taken as $v_T = \sqrt{8kT/\pi m}$. Because the particle charge must be in equilibrium, both fluxes are equal and the equation $I_e = I_i$ is solved by the Newton–Raphson method to obtain the established $U_d$ for each calculation grid cell. Also, during the afterglow simulation, the numbers of ions and electrons collected by dust are checked to verify the validity of $U_d$. This shows good applicability of such a method for calculating $U_d$.

The transport equation for the nanoparticle density $n_d(x)$, including their diffusion and drift due to the electric field and ion drag force, is solved to obtain the equilibrium dust density profile:

$$\frac{dn_d}{dt} = \frac{d}{dx}\left[D_d\frac{dn_d}{dx} + V_d(x)n_d(x)\right], \qquad (5)$$

where $D_d$ is the diffusivity of nanoparticles and $V_d(x)$ is their local average velocity, determined by the electrostatic force, ion drag force, and gas friction. The details of the dust transport model are described in [13, 14].

The obtained space charge of nanoparticles, $Z_d n_d$, is included in the Poisson equation to find the electric field in plasma.

In this paper, to take the effect of metastable states of argon atoms into account, the equation of metastable atoms kinetics is added to the described model.

## 3. METASTABLE ATOM KINETICS

Simultaneously with the discharge kinetics simulation, the balance equation for metastable argon atoms Ar* is solved. The model of metastable atom kinetics is simplified. Because argon atoms have two metastable levels with close excitation energies, they are regarded as one state with the energy offset 11.5 eV. The cross sections of the argon atom excitation to the metastable state were taken from experimental measurements [15].

We include the following main processes into the balance of metastable atoms:

a) Generation of metastable atoms Ar*, calculated in PIC–MCC simulations;

b) Diffusion of metastable atoms with a sink on the electrode surface;

c) Reaction of metastable pooling, leading to ionization:

$$\mathrm{Ar}^* + \mathrm{Ar}^* = \mathrm{Ar} + \mathrm{Ar}^+ + e;$$

d) Decay of a metastable state due to two-body Ar*–Ar collisions,

$$\mathrm{Ar}^* + \mathrm{Ar} = \mathrm{Ar} + \mathrm{Ar};$$

e) Decay of metastable state by the three-body collision mechanism,

$$\mathrm{Ar}^* + 2\mathrm{Ar} = \mathrm{Ar}_2 + \mathrm{Ar};$$

f) Metastable states quenching to resonant states by collisions with electrons:

$$\mathrm{Ar}^* + e = \mathrm{Ar}^r + e;$$

g) Stepwise ionization of metastable states by electron impact:

$$\mathrm{Ar}^* + e = \mathrm{Ar} + 2e;$$

h) Excitation of metastable states to higher-lying electron states by electron impact:

$$\mathrm{Ar}^* + e = \mathrm{Ar}^{hl} + e;$$

i) Decay of a metastable state by collision with the surface of dust particles.

The balance equation for the concentration $n^*$ of metastable atoms is written as

$$\frac{dn^*}{dt} = \frac{d}{dx}D^*\frac{dn^*}{dx} + G^* - 2K_i n^{*2} - K_{2b}n^* n_g - K_{3b}n^* n_g^2 - (K_q + K_s + K_{exc})n^* n_e - K_d n^* n_d,$$

where $G^*$ is the generation rate of metastable atoms, taken from the PIC–MCC simulation, $D^*$ is their diffusion coefficient, $K_i$ is the rate constant of metastable pooling reaction (c), $n_g$ is the gas density, $K_{2b}$ and $K_{3b}$ are the rate constants of two-body and three-body metastable state decay reactions (d) and (e), and $K_q$, $K_s$, and $K_{exc}$ are the respective rate constants of reactions of electron quenching (f), stepwise ionization (g), and excitation to higher states (h). The last term means the metastable-state decay on the dust surface, with the rate constant $K_d = \pi r_d^2 v_{T_g}$, where $r_d$ is the dust particle radius and $v_{T_g}$ is the thermal velocity of gas atoms.

The diffusion coefficient of metastable atoms was assumed to be $D^* = 2.42 \cdot 10^{18}/n_g$ cm$^2$/s, where $n_g$ is taken in cm$^{-3}$ [16]. The values of rate constants were [17, 18]

$$K_i = 6.4 \cdot 10^{-10}\ \mathrm{cm}^3/\mathrm{s}, \quad K_{2b} = 2.6 \cdot 10^{-15}\ \mathrm{cm}^3/\mathrm{s},$$

$$K_{3b} = 1.4 \cdot 10^{-32}\ \mathrm{cm}^6/\mathrm{s}.$$

The electron quenching rate constant is $K_q = 2 \cdot 10^{-7}$ cm$^3$/s for glow discharge [16], and for the

afterglow simulation, when electron temperature is low, it is taken as in [3], with exponential attenuation by the factor $\exp(-0.075/T_e)$, where $T_e$ is the electron temperature in eV and 0.075 is the energy gap between the metastable and resonant states. The values

$$K_s = 6.8 \cdot 10^{-9} T_e^{0.67} \exp(-4.2/T_e) \text{ cm}^3/\text{s},$$

$$K_{exc} = 8.9 \cdot 10^{-7} T_e^{0.51} \exp(-1.59/T_e) \text{ cm}^3/\text{s}$$

are taken from [19]. For $K_{exc}$, only the excitation to the nearest 4p state is taken into account.

## 4. SIMULATION ALGORITHM

The proposed discharge model is hybrid, combining particle simulations for the electrons and ions and solving the differential equation for the balance of metastable atoms. Kinetic equations (1) and (2) for the electron and ion energy distribution functions (EEDF and IEDF), Poisson equation (3), equations of charging of dust particles, equation of dust-particle transport (5), and the balance equation for metastable states are solved self-consistently.

The EEDF obtained from the PIC–MCC simulations provides the metastable generation rate $G^*$. The ionization in discharge now consists of two processes, the first is the electron impact on argon atoms and the second is due to reactions of metastable states. After solving the balance equation for metastable atoms at each rf cycle, new test particles are added to the PIC–MCC simulations, according to the rate of ion generation by reaction (c). Preliminary calculations have shown that for the relevant pressure and discharge voltage, neglecting the ion production by reaction (g) leaves the results practically unchanged, and therefore the additional ionization from this reaction was omitted.

In the case of a low reaction rate, if the metastable density is small, in order to avoid very small weights of test particles, the number of produced ion–electron pairs is accumulated for each grid cell during a few rf cycles until it becomes large enough to introduce a new pair of test particles with a chosen minimal weight. The new electron test particles from reaction (c) are initiated with the kinetic energy 7.3 eV, in order to conserve energy in the reaction and the isotropic velocity direction distribution. After this, the PIC–MCC simulation proceeds further.

Kinetic equations (1) and (2) are solved with the added test particles, providing a new value of metastable-state generation rate $G^*$. Other equations including the Poisson equation and dust-particle charging and transport equations are then solved with the new EEDF and IEDF. For discharge simulation, the calculations proceed until a steady solution is achieved. In the case of afterglow, the previously achieved solution is used as the initial configuration and the further evolution of plasma parameters with zero voltage on the electrodes is simulated.

## 5. MODEL OF DUST DISCHARGING

To describe the decrease in the charge of dust particles during plasma afterglow, a few simplifications were adopted. The first concerns the rate of electron desorption from the particle surface. In [6, 7], the mechanism of electron binding with a charged-particle surface was considered and attempts were made to estimate the surface binding energy and desorption rate assuming that the electron is bound to the surface by a self-induced short-range polarization potential. For a large dust particle of 4.7 $\mu$m in size, the estimate of the binding energy was on the order of 0.5 eV and the desorption rate time was less than $10^{-6}$ s. For the nanometer-size particles considered in the present model, these parameters would be even smaller. Also in [4], an estimate for the characteristic time of particle charge fluctuations is made from plasma parameters, and it has the same order of magnitude of 1 $\mu$s. Because the time scale of most of the processes in the afterglow plasma is larger, we assume that the electron desorption is fast enough for the dust particle charge to be defined at every instant by equilibrium of electron and ion fluxes.

The second simplification was to apply the OML theory expressions to calculate the dust charge, although the electron energy distribution in afterglow may be not Maxwellian. But the control of simulated electron and ion fluxes to the dust surface shows that this assumption gives sufficiently correct values of $U_d$.

In our model, during the afterglow simulation, after each fixed number of time steps, the dust floating potential $U_d$ was redefined according to OML expressions (4) using the local plasma parameters. Because the dust charge was decreasing, the electrons desorpted from dust surface were included in the simulation. First, for the calculation of the new reduced dust potential, the additional electron density $\delta n_e = -n_d r_d \delta U_d/e$ produced by desorpted electrons was included into OML expressions (4) in defining the new potential $U_d$, and hence obtaining it required iterations. Second, after converging of iterations, the final number of released electrons (known from the difference between the initial and the new approved $U_d$) was taken into the PIC–MCC simulation by introduc-

ing new electron test particles. Because the released electron must be accelerated by the repelling particle potential, the new test particle has the kinetic energy defined by the local dust potential (equal to $-eU_d$) and the isotropic velocity direction distribution. Similarly to ion–electron production in metastable pooling, to avoid very small test-particle weights, the number of desorpted electrons is accumulated in each grid cell until it becomes sufficient to introduce a new test particle. This routine was performed at each grid cell with a nonzero dust density.

## 6. RESULTS

The 13.56 MHz rf discharge was simulated in Ar at the pressure 75 mTorr, gas temperature $T_g = 300$ K, discharge voltage 150 V, and interelectrode distance $L = 3.3$ cm. Dust with a different size of the particles was added to the discharge volume. The calculations proceeded until a steady plasma parameters and metastable-atom density were obtained, which usually required up to 30000 rf cycles. The final dust density profile was close to a half-sinusoidal shape with the maximum of $2 \cdot 10^7$ cm$^{-3}$, with zero density in electrode sheaths. After this, the discharge voltage was switched off and the further evolution of plasma was simulated. For simplicity, the dust density redistribution was not considered and the density profile was held constant. The simulations of decay were limited by the first two milliseconds.

Figure 1 shows the result of discharge simulation in dust-free argon, showing the electron and ion density

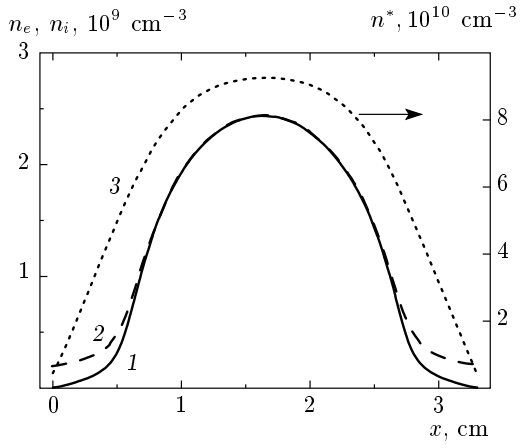


**Fig. 1.** Spatial profiles of densities of electrons $n_e$ (curve *1*), ions $n_i$ (*2*), and metastable atoms $n^*$ (*3*) in an rf discharge in argon without dust

profiles and also the metastable-atom density profile in the discharge gap. The maximal plasma density in the gap center is $2.4 \cdot 10^9$ cm$^{-3}$, the metastable-atom concentration is $9.2 \cdot 10^{10}$ cm$^{-3}$, and the electron temperature in the bulk plasma is 2.2 eV. This is the initial configuration when the voltage is switched off and simulation of afterglow is started. We also note that the ionization rate in discharge due to metastable pooling is an order of magnitude smaller than the electron–argon impact ionization rate, and it therefore affects the plasma configuration weakly.

Figure 2 shows the behavior of the electron density in the center of the discharge gap after switching off the voltage for dust-free plasma. To reveal the role of metastable atoms and also to verify the model, the decay of the same initial plasma configuration, shown in Fig. 1, was simulated twice, including and omitting the metastable effects, mainly the ionization due to metastable pooling. It can be seen from Fig. 2 that the main mechanism of plasma decay is ambipolar diffusion. For the simpler case of afterglow without metastable effect (curves *2* in Fig. 2), the characteristic time of the electron density decay can be estimated as $\tau_a = \Lambda^2/D_a$, where in one-dimensional case the diffusion length is $\Lambda = L/\pi$ ($L$ is the discharge gap equal to 3.3 cm) and the ambipolar diffusion coefficient is

$$D_a = \frac{v_{T_i}}{3n_g\sigma_{ig}}\left(1 + \frac{T_e}{T_i}\right).$$

The ion thermal velocity is $v_{T_i} = 4 \cdot 10^4$ cm/s, the gas density is $n_g = 3 \cdot 10^{15}$ cm$^{-3}$, and the ion transport cross section $\sigma_{ig}$ is of the order of $10^{-14}$ cm$^2$. At the first 0.1 ms of afterglow, the plasma decay is fast (see Fig. 2*a*) due to departure of hot electrons, but after the loss of the main part of the electron energy, for the next stage of afterglow, when the ratio $T_e/T_i$ decreases to unity, the obtained characteristic decay time for the curve *2* in Fig. 2*b* becomes about 1.25 ms, which is very close to the estimated value $\tau_a = 1.3$ ms.

The behavior of the electron temperature is shown in Fig. 3 (curve *2* for a simulation without metastables). It can be seen that after 0.3–0.5 ms after voltage switching, $T_e$ becomes practically equal to the gas temperature. This is in agreement with estimations of the electron cooling rate during afterglow in [3].

The inclusion of metastable atoms makes the behavior more complicated. The role of additional electron–ion pair production is clearly seen (curves *1* in Fig. 2). The electron density is now larger due to metastable pooling, and the decrease in the electron temperature can be divided into two stages (see curve *1* in Fig. 3). For the initial 0.1 ms, the cooling of dis-

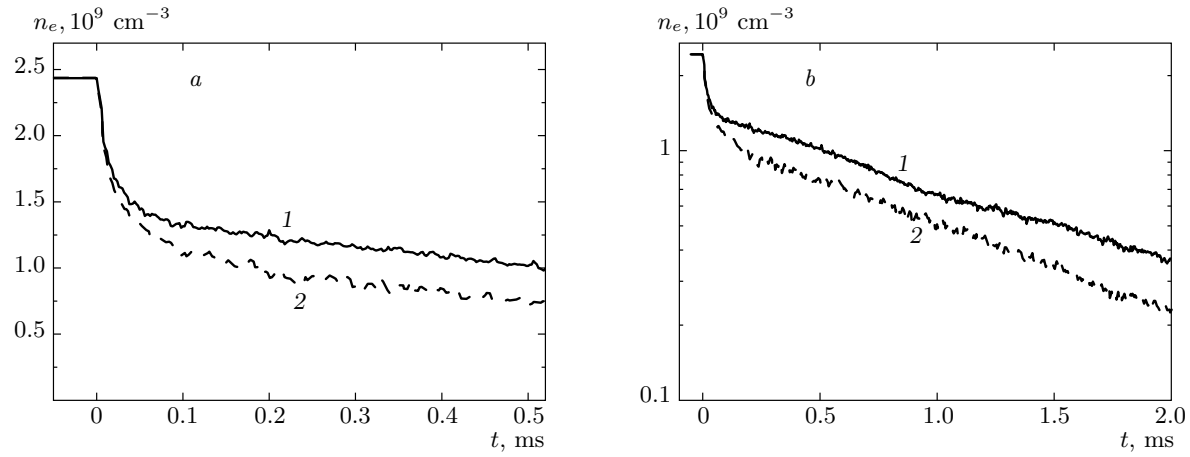


**Fig. 2.** Electron density in the discharge gap center for afterglow of a dust-free discharge plasma ($a$) for the beginning of afterglow and ($b$) for the entire simulated period. Curves *1*: simulation including metastable atom reactions; curves *2*: metastable atom reactions are omitted

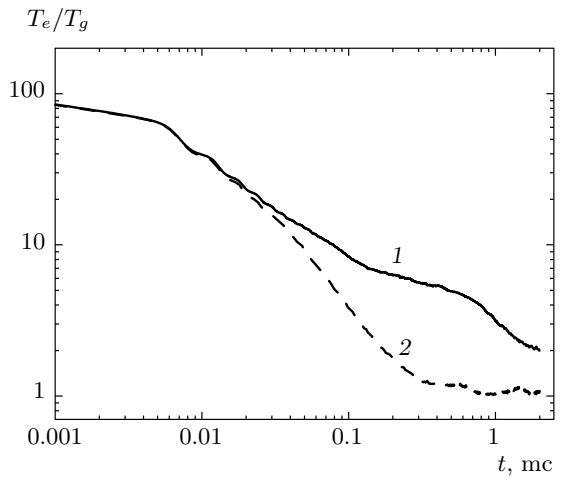


**Fig. 3.** Electron temperature normalized to the gas temperature, $T_e/T_g$, in the discharge gap center for afterglow of a dust-free discharge plasma for simulations including the metastable atom kinetics (curve *1*) and neglecting it (curve *2*)

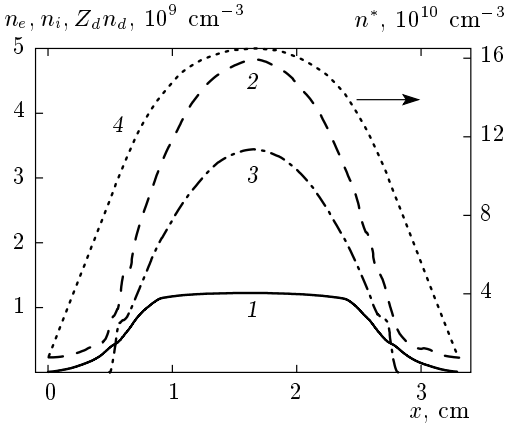


**Fig. 4.** Spatial profiles of densities of electrons $n_e$ (curve *1*), ions $n_i$ (*2*), dust space charge $|Z_d n_d|$ (*3*), and metastable atoms $n^*$ (*4*) in rf discharge containing dust particles with the radius $r_d = 50$ nm

charge plasma electrons is similar to the dashed curve, but then the effect of hot electrons with an energy of 7.3 eV, produced in metastable pooling, is noticeable. The average $T_e$ remains several times larger than $T_g$ and decreases slowly during the next millisecond, together with the decay of the density of metastable atoms, thus tending to the gas temperature. The behavior of the metastable-atom density is to be discussed below. The additional ionization and faster ambipolar diffusion partly compensate each other, and the resulting rates of density decay look similar. The anomalous increase in $n_e$ at the beginning of afterglow is not observed (Fig. 2$a$), which means that metastable pooling is not sufficient to generate it.

The next simulation corresponds to the case of a heavily dusted plasma, with the maximal dust density $n_d = 2 \cdot 10^7$ cm$^{-3}$ and with $r_d = 50$ nm. The result of discharge simulation is presented in Fig. 4. The discharge voltage was the same, but the maximal electron density was two times smaller and the electron temperature in the gap center was 3.5 eV instead of 2.2 eV in the dust-free discharge. This effect of decreasing in the electron density together with the heat-

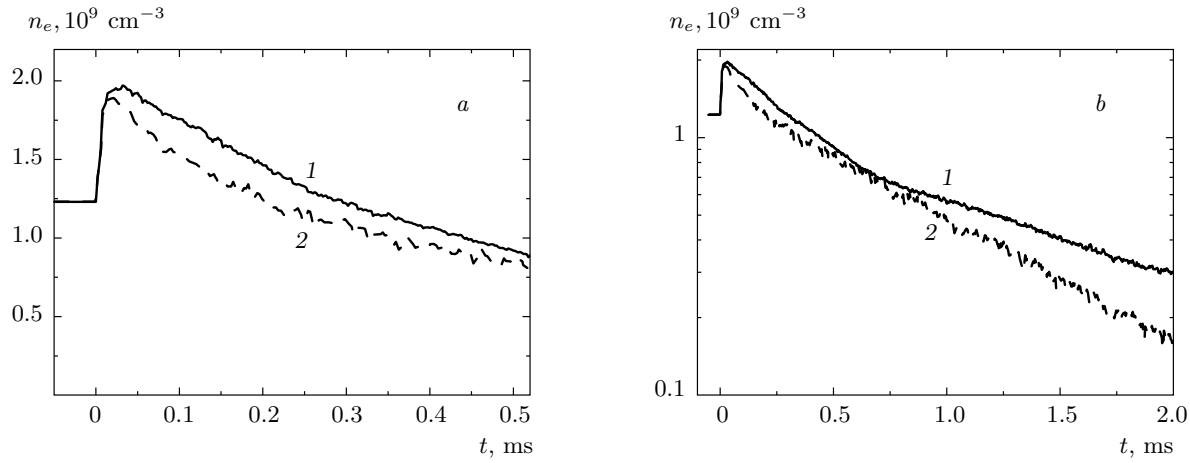


**Fig. 5.** Electron density in the discharge gap center for afterglow of discharge plasma containing dust particles with $r_d = 50$ nm ($a$) for the beginning of afterglow and ($b$) for the full simulated period. Curves *1*: simulation including metastable atom reactions; curves *2*: metastable atom reactions are omitted

ing of electrons after adding dust to the discharge is well known from experiments [20, 21] and is already described by PIC–MCC simulations [13, 14, 22]. The additional sink of electrons on the dust surface leads to depletion of their density. The electron heating due to the presence of dust is caused by a change in the electric field in the quasineutral plasma region, and the details of its mechanism are beyond the scope of this work. The metastable-atom density also increased to $1.65 \cdot 10^{11}$ cm$^{-3}$ against $9.2 \cdot 10^{10}$ cm$^{-3}$ in the dust-free case. This is in accordance with experimental observations (see, e. g., [23]), where dust contamination leads to a greater abundance of metastable atoms. The negative space charge of dust here is about three times larger than the electron density. The average charge $Z_d$ of one dust particle is near 180 in the discharge center and the dust floating potential $U_d$ is near 5 V.

Next figures show the results of the afterglow simulation for this initial plasma configuration, again performed twice, including and neglecting the effect of metastable-atom pooling. In Fig. 5, the behavior of the electron density in the gap center is shown (curves *1*: with metastable pooling, curves *2*: without it). The main difference with the dust-free plasma case is the anomalous behavior of the electron density, similar to that observed in [1]. Just after switching off the voltage, the electron density rapidly increases, similarly to the results of experiment [1]. In the framework of the model, this is explained by the loss of charge from the dust-particle surface, when the energy of electrons in the bulk plasma begins to decrease and the equilibrium dust charge, defined by the equality of electron and ion fluxes, immediately decreases, leading to intensive desorption of electrons from dust. The electron density reaches its maximum at 30–50 $\mu$s after voltage switching off and after this begins to decrease. The dust charge behavior is shown in Fig. 6. It can be concluded that the fast decrease in the dust charge during the first 50 $\mu$s of afterglow is the reason of the electron density maximum. The difference between two curves in Fig. 5 shows that the effect of metastable pooling enforces the anomalous electron density behavior, creating additional ionization. However, in the framework of the presented model, the main role in the electron density increase belongs to dust discharging. The production rate of electrons released from dust can be estimated as

$$\frac{dn_e}{dt} = -\frac{n_d r_d}{e}\,\frac{dU_d}{dt}$$

and the time derivative of $U_d$ has the same order of magnitude as the electron temperature measured in eV. This is much larger than the ionization rate of the metastable pooling reaction.

Figure 6 shows the calculated dust charge for both simulations. It can be seen that its initial decrease is independent of the effect of metastable atoms, because the first stage of electron cooling is not sensitive to metastable pooling. At the next stage of afterglow, the effect of metastable-produced ionization enlarges the dust charge due to an increase in the electron temperature (shown in Fig. 7) and also to the additional electron density.

Figure 7 shows the evolution of the electron temperature, which is close to the case of dust-free plasma,

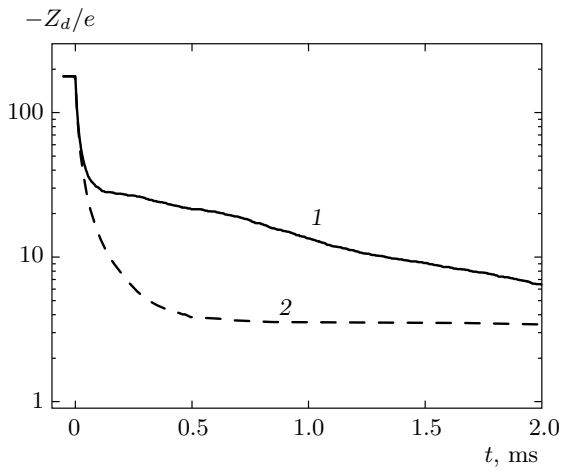


**Fig. 6.** Charge of dust particles in the discharge gap center for afterglow of discharge plasma containing dust particles with $r_d = 50$ nm for simulation including the metastable atom kinetics (curve *1*) and neglecting it (curve *2*)

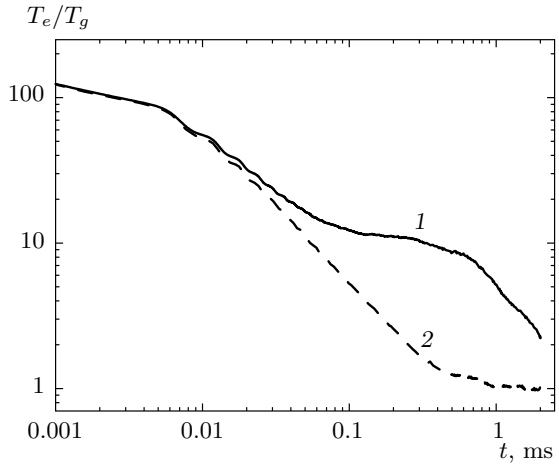


**Fig. 7.** Normalized electron temperature $T_e/T_g$ in the discharge gap center for afterglow of discharge plasma containing dust particles with $r_d = 50$ nm for simulation including metastable atom kinetics (curve *1*) and neglecting it (curve *2*)

but $T_e$ after 0.1 ms is somewhat larger due to the enhanced abundance of metastable atoms. To elucidate the behavior of $T_e$, the evolution of the EEDF in the gap center in the case with metastable pooling is shown in Fig. 8. Curve *1* in Fig. 8 for $t = 0$ corresponds to the EEDF in glow discharge. Other curves illustrates the removal of hot electrons from the plasma volume, due to their fast loss on the walls. The high-energy tail of the EEDF depletes during the first 30 $\mu$s after switching off the discharge. At the next stage of afterglow, two groups of electrons can be seen on the EEDF, the cold electrons, leaving the volume via ambipolar diffusion, and a relatively small amount of hot electrons produced by metastable pooling (curves *5* and *6* in Fig. 8).

Similarly to dust-free simulation, in the absence of the effect of metastable atoms, the electron temperature and hence the dust-particle charge become almost constant after the first 0.3–0.5 ms of afterglow and the further decay is governed by ambipolar diffusion (see dashed curves in Figs. 5–7). Here, the estimate of the electron density decay time, taking the sink on dust surface into account, must be

$$\tau_d = \left[\frac{D_a}{\Lambda^2} + n_d \pi r_d^2 v_{Ti} \left(1 - \frac{eU_d}{kT_i}\right)\right]^{-1},$$

where the first term denotes ambipolar diffusion and the second term describes the ion flux on the dust-particle surface, given by the OML theory, which is equal to the electron flux in our model. For the final stage of afterglow with a constant electron temperature, the expressions from the OML theory give $eU_d/kT_i \approx -3$ and the estimated $\tau_d \approx 1$ ms, which is in agreement with the decay time of about 0.9 ms obtained for the curve *2* in Fig. 5*b*.

The effect of metastable atoms looks similar to the one in the previous case, increasing the plasma density and maintaining the electron temperature at several $T_g$ after the first 0.5 ms of afterglow (see Fig. 7). Because the metastable density in dusty plasma is larger, the ionization from reaction (c) retards the plasma decay more efficiently and the difference of the slopes of the curves in Fig. 5*b* is more noticeable than in the dust-free case.

The next simulations were performed for a different dust-particle size, with the effect of metastable atoms included. Figure 9 shows the behavior of the electron density in the gap center during afterglow of plasma with the dust particles with $r_d$ from 10 to 50 nm. It is clearly seen that increasing the dust size enhances the anomalous electron density behavior, as was observed in experiment (shown in Fig. 7 in [1]). The maximum of the electron density during afterglow increases with the dust-particle size. To illustrate this more clearly, the densities are plotted in Fig. 9*a* only for the initial 0.2 ms of afterglow, also including the dust-free case. The discharge voltage was chosen fixed and equal to 150 V in all cases, but it is known that adding dust leads to a decrease in the electron density in discharge, and hence the initial values are different for each dust size. Besides, adding dust increases the electron tem-

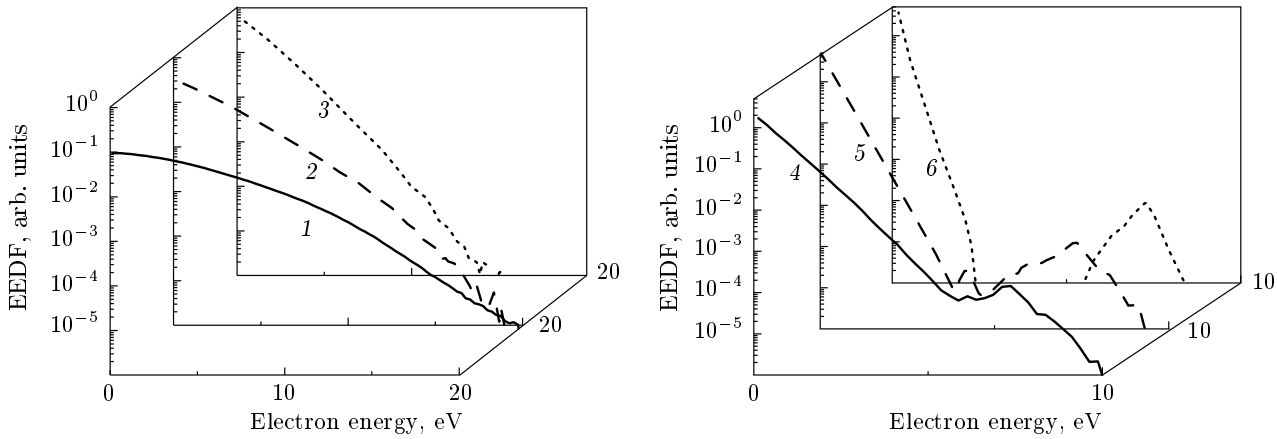


**Fig. 8.** Evolution of the electron energy distribution function in the gap center during afterglow of plasma containing dust particles with $r_d = 50$ nm at $t = 0$ (*1*), 3 $\mu$s (*2*), 10 $\mu$s (*3*), 30 $\mu$s (*4*), 150 $\mu$s (*5*), 1 ms (*6*)

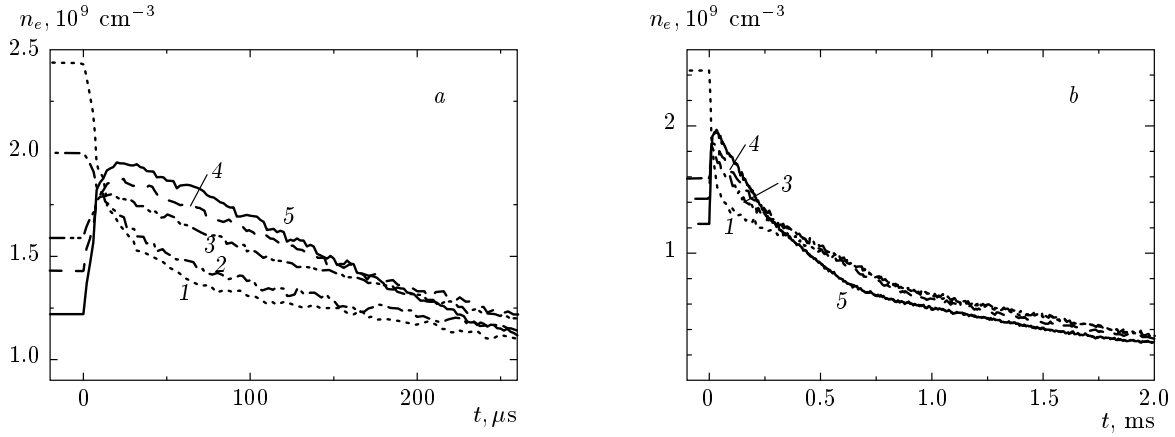


**Fig. 9.** Electron density in the discharge gap center for afterglow of discharge plasma containing dust particles with size $r_d = 10$ nm (*2*), 25 nm (*3*), 35 nm (*4*), 50 nm (*5*) (including the dust-free case, curve *1*), (*a*) for the beginning of afterglow and (*b*) for the entire simulated period

perature in the discharge bulk plasma and hence produces a larger concentration of metastable atoms, as is illustrated in the next figures. To make the results more comparable, the dust density profiles were chosen equal for all sizes, with a maximum of $n_d$ equal to $2{\cdot}10^7$ cm$^{-3}$. Figure 9*b* shows the electron density decay for the whole simulation time (we note that the curve *2* for $r_d = 10$ nm practically coincides with the dust-free one, and is therefore omitted). The enhancement of the anomalous $n_e$ behavior with the increase in dust size is due to the larger amount of released electrons.

Figure 10 shows the evolution of the dust-particle charge in the center of the gap, plotted for all considered dust sizes. The initial fast drop of charge during the first 30–50 $\mu$s is responsible for the anomalous behavior of the electron density, due to the very intense creation of desorbed electrons. We also note that after the first stage of afterglow, when electrons lose the main part of their energy, the floating dust potential $U_d$ establishes as approximately proportional to the electron temperature $T_e$: $eU_d \approx -3kT_e$.

Figure 11 show the behavior of the electron temperature. It is similar for all sizes, which shows that the electron cooling mechanism is the same during the first 0.1 ms, although the initial temperature is higher for larger dust sizes. This initial fast decrease of $T_e$, which becomes several times less during the first 30–50 $\mu$s, is the origin of the fast drop of the dust floating potential $U_d$ and hence of the dust charge, as can be seen in Fig. 10. In the time interval 0.1–1 ms, the temperature is maintained at (5–10)$T_g$ by production of hot electrons in metastable reactions. The larger

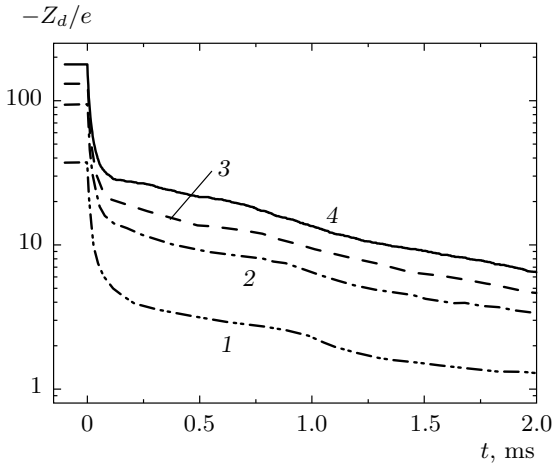


**Fig. 10.** Dust charge evolution in the discharge gap center for afterglow of discharge plasma containing dust particles with size $r_d = 10$ nm (*1*), 25 nm (*2*), 35 nm (*3*), 50 nm (*4*)

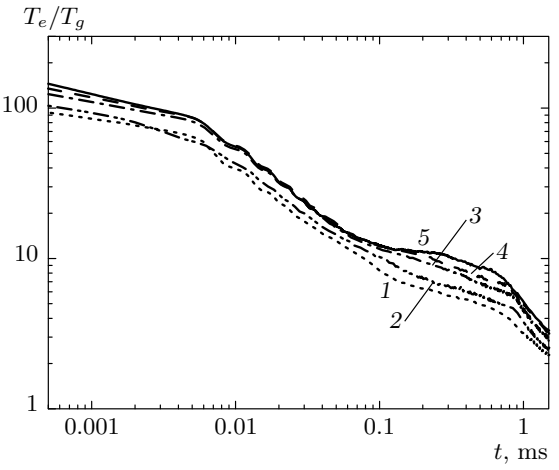


**Fig. 11.** Normalized electron temperature $T_e/T_g$ in the discharge gap center for afterglow of discharge plasma containing dust particles with size $r_d = 10$ nm (*2*), 20 nm (*3*), 35 nm (*4*), 50 nm (*5*) (including the dust-free case, curve *1*)

the size of dust particles is, the greater the abundance of metastable atoms, and hence the larger $T_e$ for this time interval. After 1 ms of afterglow, the temperature begins to decrease toward the gas temperature due to gradual depletion of the abundance of metastable atoms.

Figure 12 shows the decay of the metastable-atom density, taken in the gap center and again plotted for different dust sizes. The higher densities correspond to the larger dust contamination, which is in agreement

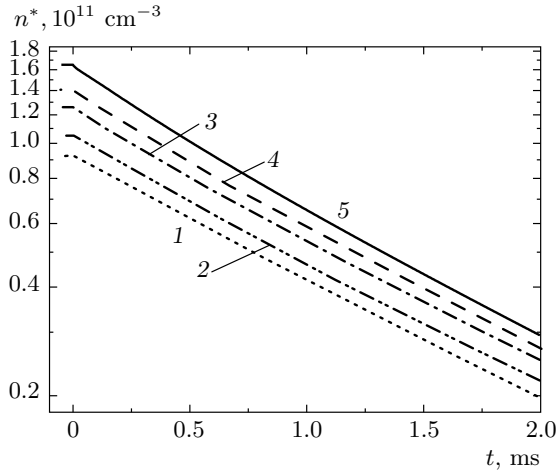


**Fig. 12.** Density of metastable argon atoms in the discharge gap center for afterglow of discharge plasma containing dust particles with size $r_d = 10$ nm (*2*), 25 nm (*3*), 35 nm (*4*), 50 nm (*5*) (including the dust-free case, curve *1*)

with experimental observations [23]. The generation of new metastable atoms practically terminates after the first 10 $\mu$s of afterglow, when $T_e$ decreases by several times.

We note that the curves in Fig. 12 are not straight and parallel as it seems. The behavior of $n^*$ is actually close to an exponential decay, but only for the simulation times longer than 0.5 ms, when metastable losses in electron reactions (f)–(h) become negligible due to the decrease in the electron temperature. Besides, the rate of pooling reaction (c) decreases as the square of the density, and hence the diffusion to the walls and collisions with dust remain the main mechanisms of the metastable-atom decay. This was already discussed in [3]. For the decay time more than 0.5 ms, the slope of curves in a logarithmic scale corresponds to

$$\tau^* = \left(\frac{D^*}{\Lambda^2} + K_d n_d\right)^{-1},$$

where the first term results from diffusion and the second accounts for the decay on dust surface. Reactions (d) and (e) of metastable atoms with gas atoms are too slow to make effect, which was also previously noted in [3].

## 7. CONCLUSION

The processes in the afterglow plasma of argon discharge containing dust were simulated by the PIC–MCC method, including kinetics of metastable atoms.

The charge of dust particles was assumed to be in equilibrium with local plasma conditions. The simulations explained the anomalous behavior of the electron density after turning off the discharge voltage by desorption of electrons from the dust-particle surface due to electron cooling. The process of afterglow can be divided into two stages: the first 0.3–0.5 ms, during which the electron temperature rapidly decreases due to energy losses, and the next one, when the electron temperature is maintained by production of hot electrons in metastable pooling reactions, gradually decreasing to the gas temperature as the metastable density is decaying. If the metastable pooling reaction is neglected, the electron temperature at the second stage of afterglow would be equal to the one of the gas.

At the beginning of the first stage of afterglow, when the electron temperature rapidly decreases, the magnitude of the floating potential of the dust surface and hence the particle charge also decrease and the electron density increases due to the intense electron desorption from the dust particles. The main production of desorbed electrons occurs during the first 30–50 $\mu$s of afterglow, when the electron temperature decreases by several times, thus producing a maximum of the electron density.

At the second stage of afterglow, as the electron temperature and dust charge decrease relatively slowly, the main mechanism of plasma decay is the ambipolar diffusion and also the sink of electrons and ions on the surface of dust particles. The decay is partially compensated by creation of additional electron–ion pairs in the metastable pooling reaction, but this does not change the electron density behavior qualitatively. The density of metastable atoms is mainly determined by diffusion to the chamber walls. At the first stage of afterglow, they are also consumed in reaction with hot electrons, but at the second stage, when the electrons are too cool to participate in reactions, the only reliable metastable-atom decay mechanism is the diffusion together with the de-excitation on the dust surface.

The results of simulation explain the anomalous behavior of the electron density in dusty plasma afterglow and show qualitative agreement with experimental observations.

This paper was supported in part by the RFBR project No. 13-02-00242 a, the bilateral RFBR–Ukraine project No. 10-02-90418, and the Integration project No. 39-2012 of the Siberian Branch of the RAS.

## REFERENCES


1. J. Berndt, E. Kovacevic, V. Selenin et al., Plasma Sources Sci. Technol. **15**, 18 (2006).
2. I. Stefanovic, J. Berndt, D. Maric et al., Phys. Rev. E **74**, 026406 (2006).
3. I. Denysenko, I. Stefanovic, B. Sikimic et al., J. Phys. D **44**, 205204 (2011).
4. A. V. Ivlev, M. Kretschmer, M. Zuzic et al., Phys. Rev. Lett. **90**, 055003 (2003).
5. L. Couedel, A. Mezeghrane, A. A. Samarian et al., Contrib. Plasma Phys. **49**, 235 (2009).
6. F. X. Bronold, H. Fehske, H. Kersten, and H. Deutsch, Phys. Rev. Lett. **101**, 175002 (2008).
7. F. X. Bronold, H. Fehske, H. Kersten, and H. Deutsch, Contrib. Plasma Phys. **49**, 303 (2009).
8. R. Lagushenko and J. Maya, J. Appl. Phys. **55**, 3293 (1984).
9. J. P. Boeuf, Phys. Rev. A **46**, 7910 (1992).
10. P. Belinguer, Phys. Rev. A **46**, 7923 (1992).
11. Yu. Chutov, O. Kravchenko, P. Schram, and V. Yakovetsky, Physica B **262**, 415 (1999).
12. V. E. Fortov, A. G. Khrapak, S. A. Khrapak et al., Uspekhi Fiz. Nauk **174**, 495 (2004).
13. I. V. Shveigert and F. M. Peeters, Pis'ma v Zh. Eksp. Teor. Fiz. **86**, 572 (2007).
14. I. V. Schweigert, A. L. Alexandrov, D. A. Ariskin et al., Phys. Rev. E **78**, 026410 (2008).
15. W. Borst, Phys. Rev. A **9**, 1195 (1974).
16. D. P. Lymberopoulos and D. J. Economou, J. Appl. Phys. **73**, 3668 (1993).
17. C. M. Ferreira, J. Loureiro, and A. Ricard, J. Appl. Phys. **57**, 82 (1985).
18. K. Tachibana, Phys. Rev. A **34**, 1007 (1986).
19. S. Ashida, C. Lee, and M. A. Lieberman, J. Vac. Sci. Technol. A **13**, 2498 (1995).
20. P. Belenguer and J. P. Boeuf, Phys. Rev. A **46**, 7923 (1992).
21. J. Berndt, E. Kovacevic, I. Stefanofic et al., Contrib. Plasma Phys. **49**, 107 (2009).
22. W. J. Goedheer, V. Land, and J. Venema, J. Phys. D **42**, 194015 (2009).
23. I. Stefanovic, N. Sadeghi, and J. Winter, J. Phys. D **43**, 152003 (2010).